Evolution of the Solid−Electrolyte Interphase on Carbonaceous Anodes Visualized by Atomic-Resolution Cryogenic Electron Microscopy

William Huang,[†] Peter M. Attia,[†] Hansen Wang,[†] Sara E. Renfrew,[‡,§] Norman Jin,[†]
Supratim Das,[⊥] Zewen Zhang,[†] David T. Boyle,[∥] Yuzhang Li,[†] Martin Z. Bazant,[⊥]
Bryan D. McCloskey,[‡,§] William C. Chueh,*[,†,#] and Yi Cui*[,†,#]

[†]Department of Materials Science and Engineering, Stanford University, Stanford, California 94305, United States

[‡]Energy Storage and Distributed Resources Division, Lawrence Berkeley National Laboratory, Berkeley, California 94720, United States

[§]Department of Chemical and Biomolecular Engineering, University of California, Berkeley, California 94720, United States

[∥]Department of Chemistry, Stanford University, Stanford, California 94305, United States

[⊥]Department of Chemical Engineering, Massachusetts Institute of Technology, Cambridge, Massachusetts 02139, United States

[#]Stanford Institute for Materials and Energy Sciences, SLAC National Accelerator Laboratory, 2575 Sand Hill Road, Menlo Park, California 94025, United States

S *Supporting Information*

ABSTRACT: The stability of modern lithium-ion batteries depends critically on an effective solid−electrolyte interphase (SEI), a passivation layer that forms on the carbonaceous negative electrode as a result of electrolyte reduction. However, a nanoscopic understanding of how the SEI evolves with battery aging remains limited due to the difficulty in characterizing the structural and chemical properties of this sensitive interphase. In this work, we image the SEI on carbon black negative electrodes using cryogenic transmission electron microscopy (cryo-TEM) and track its evolution during cycling. We find that a thin, primarily amorphous SEI nucleates on the first cycle, which further evolves into one of two distinct SEI morphologies upon further cycling: (1) a compact SEI, with a high concentration of inorganic components that effectively passivates the negative electrode; and (2) an extended SEI spanning hundreds of nanometers. This extended SEI grows on particles that lack a compact SEI and consists primarily of alkyl carbonates. The diversity in observed SEI morphologies suggests that SEI growth is a highly heterogeneous process. The simultaneous emergence of these distinct SEI morphologies highlights the necessity of effective passivation by the SEI, as large-scale extended SEI growths negatively impact lithium-ion transport, contribute to capacity loss, and may accelerate battery failure.
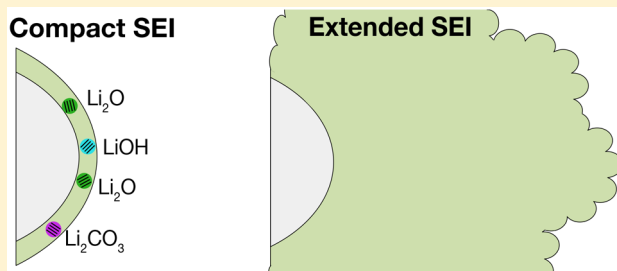
KEYWORDS: *Lithium-ion batteries, transmission electron microscopy, cryogenic electron microscopy, solid−electrolyte interphase, carbon anode*

State-of-the-art lithium-ion batteries rely on carbonaceous negative electrodes. The functionality of these electrodes strongly depends on the physicochemical properties of the solid−electrolyte interphase (SEI), a passivating layer that forms on the surface of almost all lithium-ion battery negative electrodes as a result of electrochemical decomposition of the electrolyte. While a well-passivating SEI is necessary to kinetically inhibit the electrochemical electrolyte reduction, its continuous formation consumes cyclable lithium and thus reduces battery lifetime.[1−8] SEI growth can also impede lithium-ion transport on the particle[9] and electrode[10−15] length scales, which can trigger undesirable parasitic reactions such as lithium plating and hasten battery failure.[2,11] Given the importance of the SEI to battery performance, the SEI on

carbon electrodes has been extensively characterized via physical and chemical methods such as X-ray photoelectron spectroscopy (XPS), mass spectrometry, and Fourier-transform infrared spectroscopy.[5,7,8,16−27] However, SEI characterization remains challenging due to its nanoscale morphology,[5,8,28] complex and multicomponent chemical composition,[8,29−31] reactivity to oxygen and moisture,[5,29,32,33] and sensitivity to X-ray and electron radiation.[29,34,35] Employing atomic-resolution characterization techniques that overcome
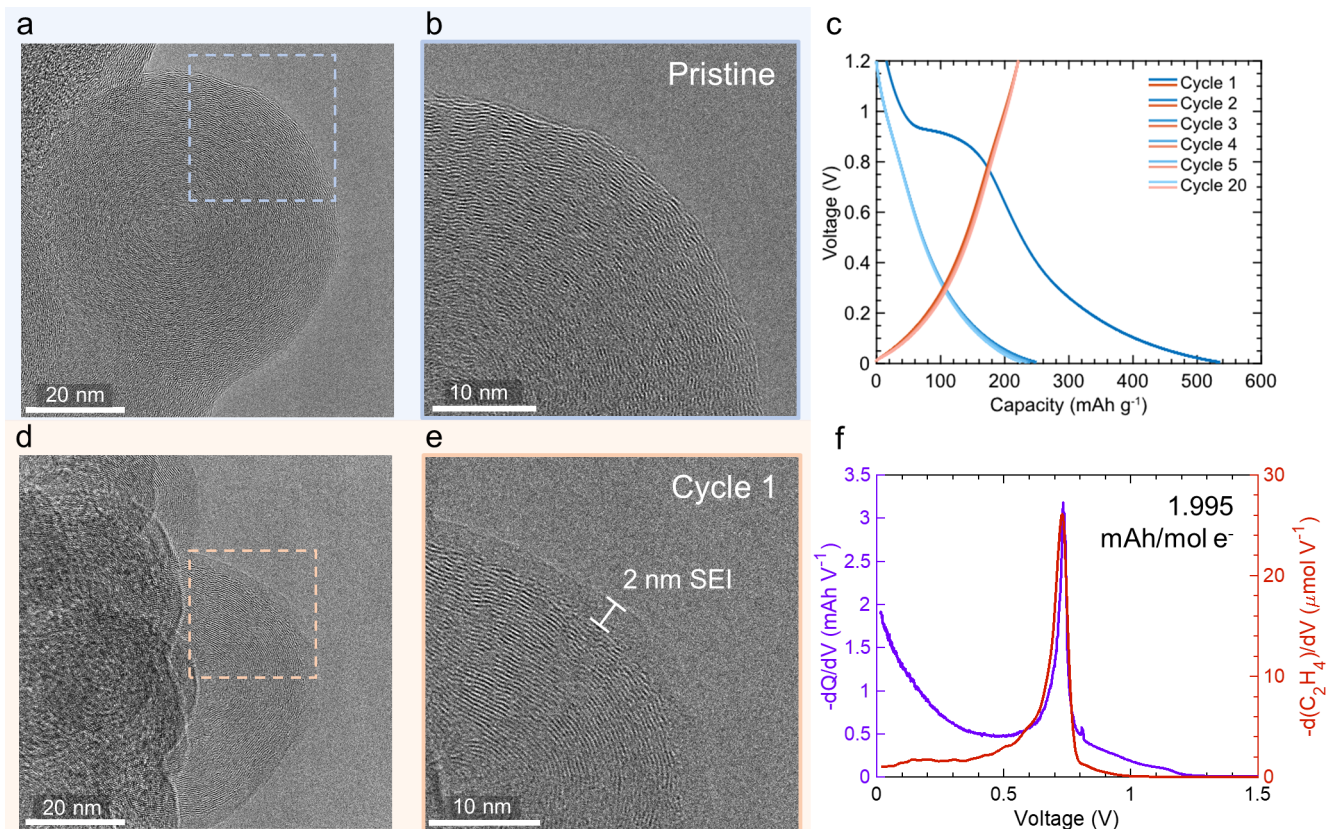
Figure 1. Initial formation of SEI on carbon black. (a, b) Cryo-TEM images of pristine carbon black. The {001} planes are readily visible. (c) Voltage−capacity curves of a carbon black/Li half-cell cycled at C/10. Lithiation and delithiation are represented by blue and red curves, respectively. Reproduced with permission from ref 40. Copyright 2019 The Electrochemical Society. (d, e) Cryo-TEM images of the SEI formed on carbon black in the delithiated state after 1 cycle. The approximate SEI thickness is 2 nm (Table S1). Fast Fourier transforms (FFTs) are available in the Supporting Information. (f) dQ/dV and ethylene gas signal detected via DEMS as a function of voltage for the first lithiation of a carbon black/Li cell cycling at C/10. The ethylene gas peak tracks to the voltage plateau at ∼0.8 V; gas is not generated at lower potentials.

these obstacles is necessary to deepen our understanding of the structure and function of this complex interphase.

Recent advances in cryogenic electron microscopy (cryo-EM) have enabled atomic-resolution imaging of air- and radiation-sensitive battery components, specifically the SEI on the metallic lithium[29,36−38] and oxidized copper.[39] Previous work has revealed the diversity of nanostructures present in the SEI on Li metal, exhibiting both layered[30] and mosaic[31] structural motifs. While this powerful technique has unlocked novel insights into the mechanisms of Li metal deposition and SEI growth, cryo-EM has yet to be applied to study the SEI that forms on carbon negative electrodes, as well as how this SEI evolves with cycling. The application of cryo-EM to study SEI growth beyond the first cycle can reveal the morphological and chemical evolution of the SEI on carbonaceous negative electrodes under different operating conditions.

In this work, we use *ex situ* cryo-EM to track the structural and chemical evolution of the SEI on carbonaceous negative electrodes during cycling. We select carbon black as a model carbon nanomaterial with which to study SEI growth and evolution due to its graphitic structure,[40,41] high surface area, electron transparency, and well-defined {001} planes.[40] We find that, after significant cycling, well-passivated particles grow a highly inorganic "compact" SEI on the order of 5 nm, while other poorly passivated particles form an "extended" SEI consisting of alkyl carbonates that can extend hundreds of nanometers. This extended SEI is a principal consumer of

lithium ions, and its large length scale causes a readily observed decrease in electrode porosity. This loss of porosity likely increases the overpotential for lithium-ion transport in the electrolyte and may lead to capacity fade and lithium plating. SEI growth on the order of hundreds of nanometers has been previously detected by tomography[13] and pressure measurements,[15] but cryo-EM provides a unique view into its structure and chemistry. Furthermore, the variable SEI thicknesses illustrates the highly heterogeneous nature of SEI growth after significant aging. This work reveals the heterogeneity of SEI formation and evolution on carbon electrodes and the utility of cryo-EM for nanoscale characterization of the chemistry and morphology of the SEI.

Carbon black is a model carbonaceous negative electrode material for the microscopic and electrochemical study of SEI growth as well as a commonly used conductive additive in commercial lithium-ion battery electrodes. The basal/edge plane structure of carbon black is similar to graphite,[40] and its structure is ideal for TEM imaging due to its small size (∼50 nm) and well-aligned {001} planes (Figure 1a,b). The {001} planes are clearly visible at the particle edge regardless of particle orientation due to spherical symmetry, making the electrode/SEI interface easily distinguishable. Furthermore, the high specific surface area of carbon black (∼62 m^2 g$^{−1}$) results in a large nominal SEI irreversible capacity, which enables facile electrochemical characterization of SEI growth.[40] Voltage−capacity curves of carbon black/lithium half-cells in
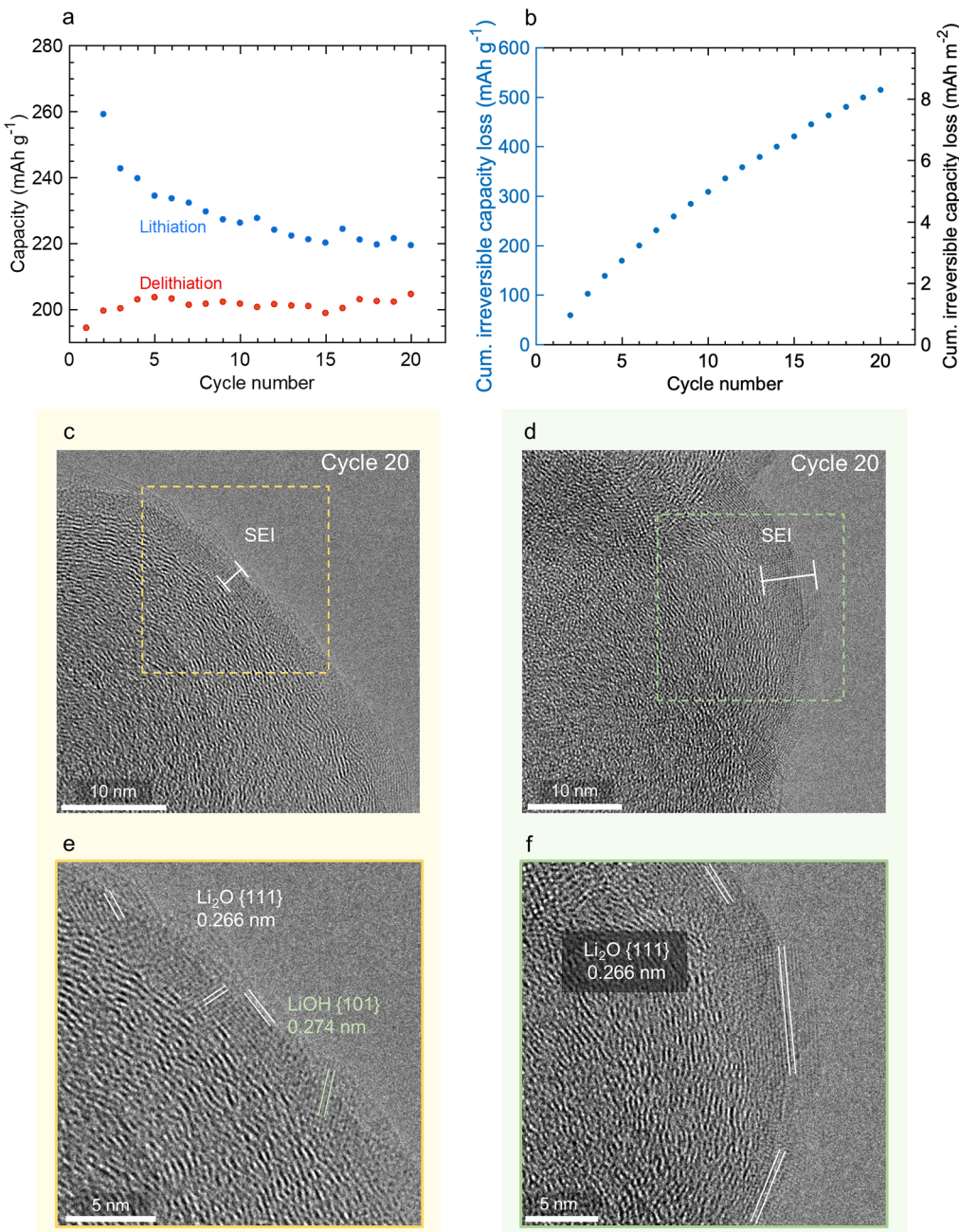
Figure 2. Evolution of the compact SEI with cycling. (a) Lithiation and delithiation capacities of the carbon black electrode during cycling. (b) Cumulative irreversible capacity loss of the carbon black electrode during cycling, excluding the first-cycle irreversible capacity. (c−f) Cryo-TEM images of the late-cycle compact SEI directly interfaced with the carbon particle after 20 cycles. The approximate SEI thickness is 5 nm (Table S1). Fast Fourier transforms (FFTs) are shown in the Supporting Information.

ethylene carbonate/diethyl carbonate (EC/DEC) with 1.0 M LiPF$_6$ electrolyte cycled at C/10 with a cutoff voltage of 10 mV (versus Li/Li$^+$) are displayed in Figure 1c, where 1 C represents 200 mA g^{-1}. With the exception of the first lithiation, no plateaus are observed in the voltage profiles, indicating a suppression of graphitic phase separation[42−44] as previously confirmed by *in situ* X-ray diffraction.[42] This difference in electrochemistry between carbon black and graphite may lead to differences in SEI growth. The lithiation capacities decrease with cycling, while the delithiation capacities are constant; this trend suggests that the SEI primarily grows during lithiation.[40] Notably, the first cycle exhibits a large voltage plateau at ∼0.9 V at C/10,

corresponding to the onset of ethylene carbonate decomposition and initial SEI formation. The total capacity of the first lithiation exceeds 500 mA h g^{-1}, because of the unique first-cycle SEI formation reaction.[4,7,45]

Representative micrographs of the carbon surface and the initial SEI after the first lithiation are displayed in Figure 1d,e. We observe a thin (∼2 nm), primarily amorphous SEI layer directly interfaced with the carbon black {001} planes (see Table S1 for precise quantification). We note that particles soaked in electrolyte for many weeks in the delithiated state do not exhibit an SEI layer (Figure S1), confirming that the SEI observed after cycling is not an artifact of sample preparation or residual electrolyte. In general, this thickness of the newly
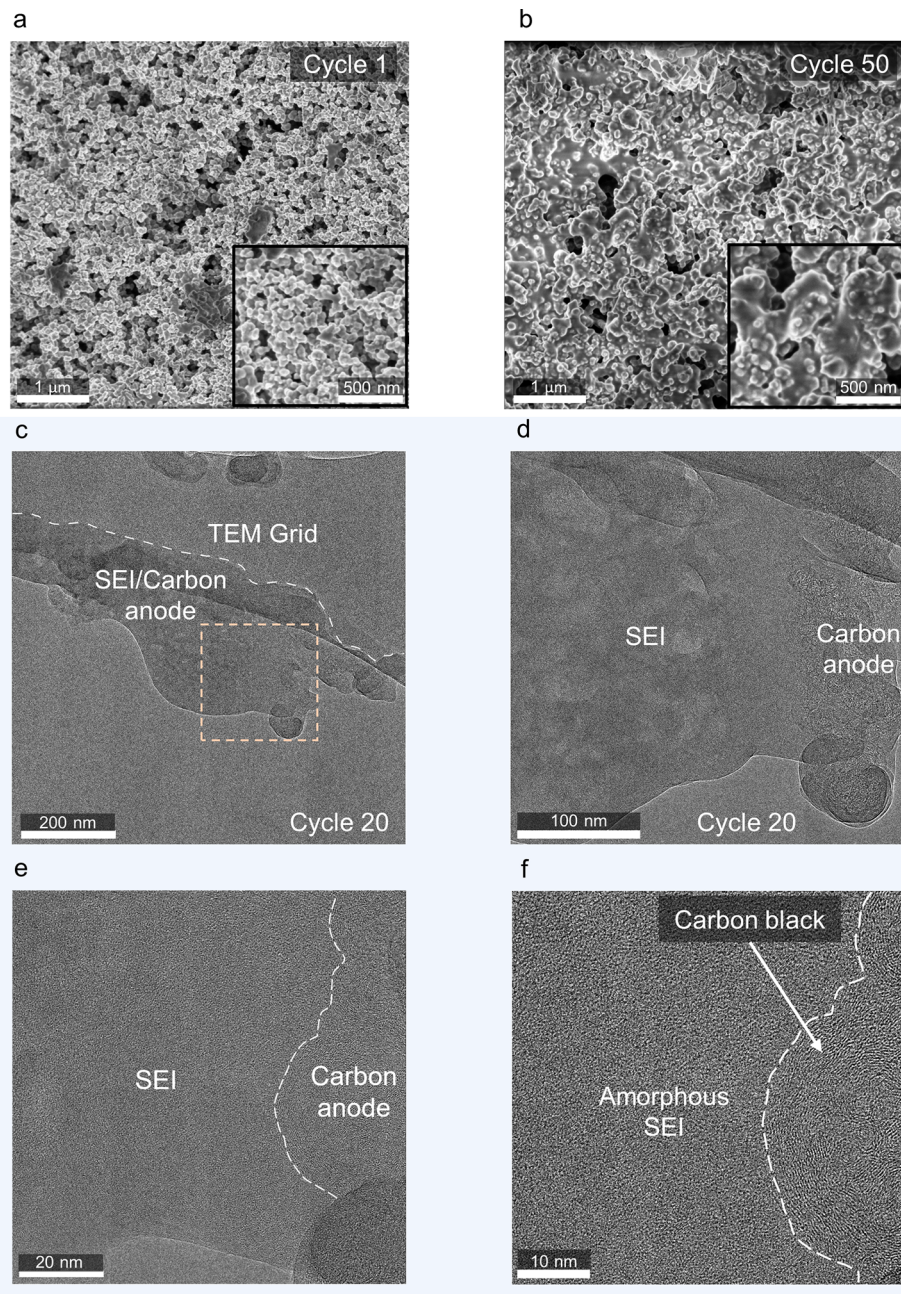
Figure 3. Emergence of an extended SEI with cycling. (a) SEM of a cross-sectioned electrode on the 1st cycle with individual carbon particles still distinguishable. (b) SEM of a cross-sectioned electrode on the 50th cycle with many carbon particles obscured by large SEI deposits. (c, d) Bright-field cryo-TEM of large extended SEI deposits spanning hundreds of nanometers. (e, f) Cryo-HRTEM of the extended SEI interfaced with carbon black. Fast Fourier transforms (FFTs) are available in the Supporting Information.

formed SEI is consistent with commonly proposed rate-limiting steps of SEI growth such as electron tunneling.[46,47] The carbon black crystalline surface appears identical to the pristine particle, suggesting that SEI growth does not alter the surface. We also note that larger extended SEI growths (∼40 nm) are occasionally visible after only the first cycle (Figure S2).

We perform differential electrochemical mass spectrometry (DEMS) to better understand the chemical composition of this nascent SEI (Figure 1f). Significant ethylene gas is evolved during the voltage plateau in the first cycle through a two-electron reduction (Figure S3), while other gases were not detected. The composition of the evolved gas suggests that

lithium ethylene dicarbonate (LEDC), likely formed from the reduction of ethylene carbonate via $2EC + 2e^- + 2Li \rightarrow (CH_2OCO_2Li)_2 + CH_2{=}CH_2$,[48,49] is the principal organic component of the SEI. The ethylene gas evolution ceases after the first lithiation (Figure S4). This result is consistent with previous work studying gas evolution on graphite electrodes.[48,50−53]

We then study the evolution of the SEI after significant cycling. The lithiation and delithiation capacities of a carbon black half-cell cycled at C/10 for 20 cycles are displayed in Figure 2a. We choose a low cycling rate to minimize transport gradients within the electrode, as the capacity at rates below C/5 is identical.[40] Figure 2b displays the cumulative

D
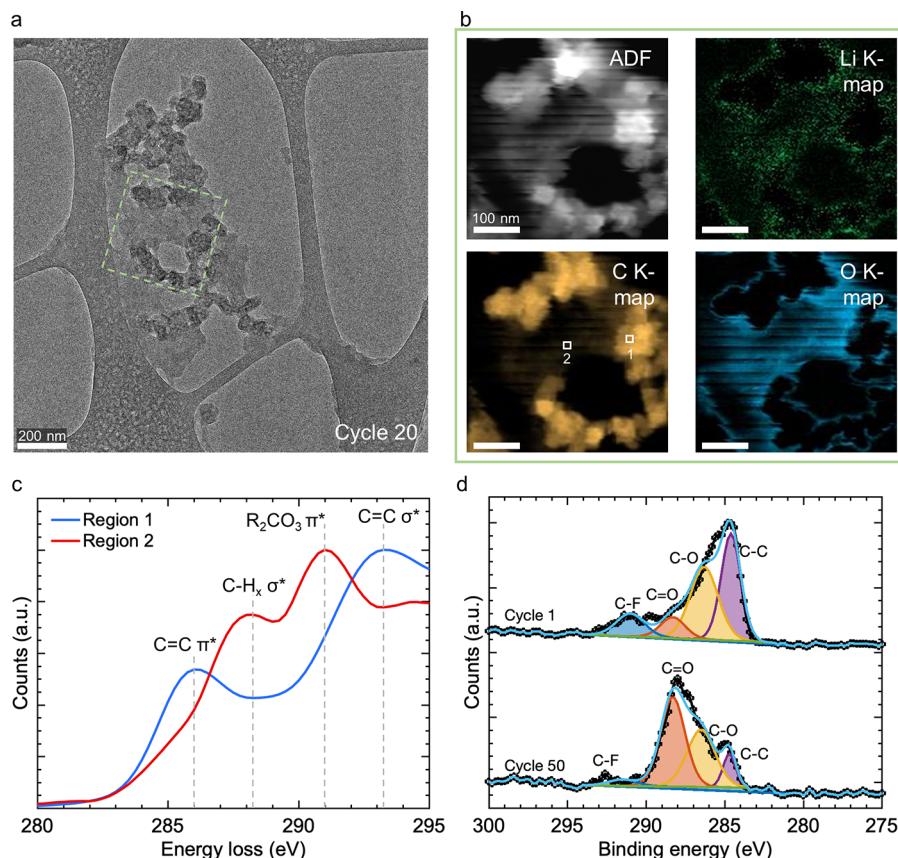
Figure 4. Chemical analysis of the extended SEI. (a) Bright-field cryo-TEM of a region of an extended SEI interfaced with carbon particles. A fast Fourier transform (FFT) is available in the Supporting Information. (b) Dark-field cryo-STEM and cryo-STEM-EELS maps of the region outlined in part a. (c) C K-edge fine structure of Region 1 and Region 2 indicated in part b. (d) XPS characterization of the electrode surface after 2 min of Ar sputtering to remove residual electrolyte. Depth profiles are shown in the Supporting Information, and increased C=O counts after 50 cycles are observed regardless of sputter time. The binding energy is calibrated to the adventitious carbon peak.

irreversible capacity loss (excluding the first cycle), estimated by subtracting the lithiation capacities from the delithiation capacities. This approach is reasonable for half-cells cycled at low rates (i.e., with small overpotentials). The cumulative irreversible capacity from cycles 2 to 20 exceeds 8 mA h m^{-2}, or 500 mA h g^{-1}, which is more than double the measured reversible capacity of carbon black. This large irreversibility is reasonable given the high specific surface area of carbon black; however, the continuous increase in irreversible capacity indicates that the first-cycle SEI growth does not effectively passivate the electrode, and further electrochemical reactions take place as the SEI continues to form. The irreversible capacity loss versus time is displayed on a log–log plot in Figure S5.

After 20 cycles at C/10, we observe two vastly contrasting morphologies of SEI growth: a compact SEI on the order of 5 nm (Figure 2), and an extended SEI on the order of 100 nm (Figures 3 and 4). Our observation of distinct compact and extended SEI layers is similar to that presented by Edstrom[28] and Peled;[8] however, we find that these layers occur on separate particles, instead of both layers occurring on the same particle.

Representative micrographs of the compact SEI in the delithiated state after cycling are presented in Figure 2c−f. Again, the carbon black crystalline surface does not appear to be damaged by SEI growth. We observe that the initial SEI further evolves into a compact SEI that approximately doubles

in thickness to ∼5 nm (Table S1) and is consistent with a simple geometric estimate of capacity loss (see the Supporting Information). This compact SEI has a high concentration of crystalline inorganic components including Li$_2$O and LiOH, distributed in an amorphous matrix. Li$_2$CO$_3$ is also observed in the compact SEI (Figure S6). This nanostructure suggests the mosaic structure of the SEI originally proposed by Peled[31] and consistent with previous cryo-EM characterizations of SEI grown in ethylene carbonate-based electrolytes on metallic lithium and oxidized Cu.[29,38,39] Notably, crystalline LiF does not appear to be a key component of the compact SEI; recent work has shown that LiF precipitates as nanoparticle agglomerates onto the surface of the negative electrode rather than incorporating within the compact SEI.[54] Inorganic SEI components such as Li$_2$O are products of ethylene carbonate decomposition because of the continuous cycling of the carbon negative electrode to low potentials versus Li/Li$^+$,[17,39,55] while components such as LiOH may result from trace water contamination in the electrolyte.[4] These species are expected to be effective in negative electrode passivation because of their electronic insulation and high dielectric constant and may be key to the stability of the carbonaceous negative electrode.

In addition to a compact SEI, we also observe an extended SEI that spans a much larger length scale. Through *ex situ* scanning electron microscopy (SEM) of a cross-sectioned electrode, we observe that significant morphological changes take place over battery cycling beyond the growth of a compact

SEI (Figure 3a,b). While the carbon electrode after the initial cycle is covered in a thin layer of SEI, individual particles remain distinguishable, and the porosity of the electrode is maintained. After many cycles, a thick, binding SEI extends among many electrode particles, concurrent with the previously observed compact SEI. This extended SEI significantly reduces the electrode porosity, increasing the overpotential for electrolyte transport.

Using cryo-EM, we probe the nanostructure of this late-cycle extended SEI and its interface with carbon. Here, we study binder-free electrodes to avoid convolution of the SEI with binder. Diffraction contrast in bright-field cryo-TEM from the carbon black {001} planes shows carbon particles at the edges of the structure, interfaced with a central amorphous region extending hundreds of nanometers (Figure 3c,d). Notably, this large (~100 nm), amorphous SEI extends beyond the length scale of the previously observed compact SEI, suggesting that this may be the porous, electronically insulating extended SEI proposed in late-stage SEI growth models.[8,9,56] Peled et al.[57] previously reported that a large, porous SEI predominantly grows on basal surfaces in graphitic electrodes; thus, carbon black's high availability of basal planes may lead to extensive extended SEI growth. We also examine these extended SEI growths using microscopy techniques including SEM and atomic force microscopy (AFM) (Figures S7−S9) for a more complete picture of the morphology of this extended SEI; the extended SEI generally encapsulates the carbon black particles. The morphology of the extended SEI is clearly visible via SEM and AFM on particles harvested from cycled electrodes, but not on pristine or electrolyte-soaked particles (Figures S10−S14). Again, both Figure 2c−f and Figure 3c−f are cycled under the same conditions for approximately 20 cycles, indicating two concurrent pathways of SEI growth.

Cryogenic high-resolution TEM (cryo-HRTEM) imaging of the SEI/carbon black interface shows the well-defined carbon black {001} planes; however, no carbon black is observed within this amorphous, extended SEI (Figure 3e,f), suggesting that our observation is not due to structural disintegration of the active material. Likewise, the extended SEI is unrelated to the binder as it is observed in electrodes with and without binder. Cryo-HRTEM characterizations of the well-passivated, compact SEI on carbon in Figure 2c−f show significant crystalline reflections from inorganic SEI components such as Li_2O or LiOH, whereas the carbon black/extended SEI interface does not contain crystalline components. This observation suggests that these inorganic crystalline SEI particles may be the key components of effective passivation by compact SEI, and their absence at the extended SEI/carbon interface may lead to poor passivation. These passivating characteristics may be attributed to their electronic properties, such as their intrinsically low conductivity and high dielectric constant preventing electron transfer, or their high elastic modulus mechanically stabilizing the SEI.[58,59]

The simultaneous emergence of the ~5 nm compact SEI and ~100 nm extended SEI on cycled electrodes suggests particle-level heterogeneity in SEI growth; rather than the extended SEI growing on top of the compact SEI, the extended SEI grows simultaneously with the compact SEI on independent particles. While heterogeneous SEI growth has been widely reported,[25,60,61] the extent of heterogeneity revealed by cryo-TEM is significant and surprising. Differences on the electrode level, such as depth within the porous electrode, cannot be responsible for this result due to the low

cycling rates applied; SEM cross sections of the electrode confirm this result (Figure S15). Additionally, small differences in the first-cycle SEI formed on different particles may lead to significant differences in the SEI that evolves upon further electrode aging. Understanding the origin of these differences is critical to control the evolved SEI morphology and motivates *in situ* studies to track SEI evolution on individual particles within the porous electrode.

In addition to structural information accessed through bright-field and HRTEM, rich chemical information can be obtained through cryogenic scanning TEM (cryo-STEM) electron energy loss spectroscopy (EELS) with high spatial resolution. Cryo-STEM-EELS mapping of the extended SEI region in Figure 4a yields the annular dark-field (ADF) image, along with the Li K-map, C K-map, and O K-map of Figure 4b. The off-axis ADF detector shows high intensity from the carbon black particles due to their crystalline nature, which is further supported by the carbon K-map. High carbon counts are attributed to the pure carbon from the carbon black, while the extended SEI shows a lower carbon signal relative to the carbon electrode. The Li K-map shows uniform Li distribution throughout the extended SEI, suggesting that the extended SEI consists mainly of lithium-containing components. We measure low lithium intensity in the carbon black particles as the sample was prepared in the delithiated state; this result also confirms that lithium does not become inaccessible within carbon black and suggests that the SEI is the dominant capacity-loss mechanism in this system. The O K-map shows significant oxygen within the extended SEI. We note that the fluorine EELS signal is weak in the extended SEI (Figure S16).

EELS fine structure analysis of the carbon K-edge offers insight into the bonding environment of carbon molecules within the SEI (Figure 4c). Whereas the C fine structure of the carbon black region (Region 1) shows bonding indicative of the C—C bonds characteristic to pristine carbon black (Figure S17), the C fine structure within the SEI differs significantly. The SEI C fine structure is dominated by the peaks at 288 and 291 eV, indicative of C—H bonding and carbonate groups, respectively.[62] This bonding environment and amorphous structure of these extended SEI regions implies an organic composition. This result suggests that the extended SEI consists of alkyl carbonates and is consistent with conventional SEI chemical analysis techniques such as air-free XPS, which show increased C=O signal on late cycle (Figure 4d), albeit with significantly lower in-plane spatial resolution. In XPS, the relative intensities of all noncarbonate peaks are suppressed for the late-cycled electrode due to the emergence of the C=O signal, likely from the extended SEI. Only via techniques with high in-plane spatial resolution, such as cryo-STEM-EELS, can the origin of this increased carbonate signal be pinpointed and attributed to the extended SEI.

These findings may also have implications for SEI growth in the crucial first cycle, during the initial "forming" of the battery. The observation of ethylene gas release during the first cycle suggests the initial formation of organic products, such as LEDC, in common with the extended SEI, over at least part of the pristine electrode surface. Coupled with our observation of spatial heterogeneity in the late-state SEI between regions dominated by the compact and extended SEI, this result suggests that competing electrochemical reactions in the first cycle lead to heterogeneous patterns of inorganic and organic products, which serve to nucleate the compact and extended SEI in different locations. The desirable slow transition of the
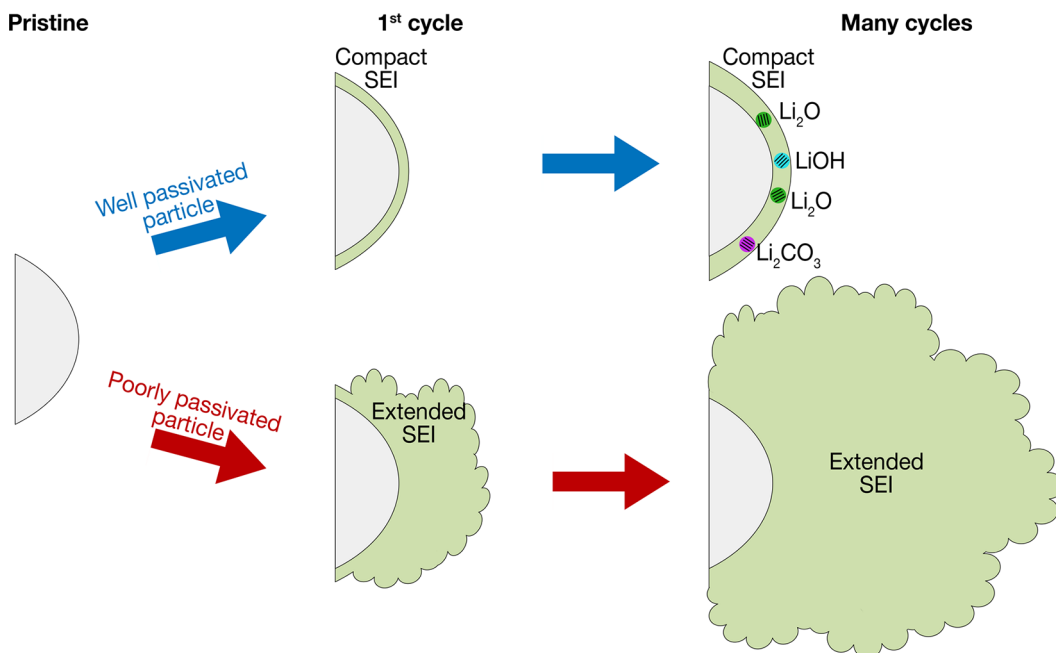
Figure 5. Schematic of SEI formation on the carbon negative electrode. As the carbon particles are lithiated during the first cycle, a thin, initial SEI is formed. After significant aging via cycling, some carbon particles form an efficient, passivating compact SEI that contains inorganic components such as Li_2O. However, other particles form extended SEI growths extending hundreds of nanometers, possibly from ineffective formation of a compact SEI. This extended SEI is the principal consumer of lithium ions.

compact to extended SEI may thus be circumvented in some locations, leading to early growth of the extended SEI and faster capacity fade. A promising strategy to extend battery lifetime, therefore, may be to select or modify pristine electrode surfaces and electrolyte components to favor compact SEI reactions in the first cycle.

Growth of this extended SEI is a major source of capacity loss within the battery. While an ideal SEI is expected to passivate within a few nanometers of the electrode, this observation of an SEI extending hundreds of nanometers on some particles indicates that the SEI does not always provide good passivation. Given its size, the growth of this extended SEI is unlikely to be limited by electron transport. Here, we analyze three hypotheses to explain this surprising result.

First, we consider electrolyte molecule transport through the extended SEI. Electrolyte molecule transport, specifically solvent molecule transport, is a commonly proposed mode of long-term SEI growth.[9,47,56,63,64] Given the amorphous morphology of the extended SEI and the lack of inorganic components at the carbon/SEI interface, solvent may be able to transport either through nanoscale pores in the extended SEI or through the polymeric network if swollen with electrolyte. AFM of particles with an extended SEI reveals a smooth surface (Figure S9), suggesting that pore sizes are at least smaller than the AFM probe size (10 nm).

To gauge the feasibility of this pathway, we use a simple model[9] to estimate the electrolyte diffusivity in the extended SEI (see the Solvent Diffusivity Estimation section in the Supporting Information). The diffusivity is approximately 10^{-15} cm^2 s^{-1}, which is generally in good agreement with the literature. Thus, our observations are quantitatively consistent with the hypothesis of extended SEI growth limited by solvent/electrolyte transport.

Another possible pathway for growth of the extended SEI is the continued reaction and precipitation of radicals generated during SEI nucleation. During initial SEI formation, the reduction of electrolyte molecules forms highly reactive radicals, some of which remain in the liquid phase and can continue to react in the electrolyte, precipitating their reaction product on the negative electrode at later stages.[65−68] These radicals may propagate easily through organic layers such as a compact SEI lacking crystalline SEI components, which is consistent with our observation of extended SEI growth on carbon black without a crystalline compact SEI. The majority of these radicals is formed on the first cycle, and thus, instances of smaller extended SEI precipitation are observed even on the first cycle (Figure S2). In this scenario, the evidence for electrochemical SEI growth observed in Figure 2a,b and previously is explained by the growth of a compact SEI, while extended SEI growth via radical formation would not be detected electrochemically.

A third possibility is that this extended SEI may result from precipitation of soluble SEI species.[35] The compact SEI formed on the negative electrode consists of insoluble SEI species; however, as electrolyte is consumed through SEI growth, the concentration of the soluble SEI increases and may precipitate back onto the negative electrode as electrolyte continues to be consumed. The precipitation of this soluble SEI may be preferential on poorly passivated particles without inorganic SEI components. In this pathway, SEI growth proceeds via normal electrochemical and chemical routes, reflected in electrochemical measurements, and the extended SEI is formed via this distinct precipitation process. This effect could also be a purely chemical phenomenon or a corrosion process, involving locally coupled reduction and oxidation reactions that do not transfer net electrons through the external circuit.[69] However, both the relatively high electrolyte volumes used in our cells and the well-defined interface observed between the extended SEI and carbon black suggest that this hypothesis is unlikely.

Growth of the extended SEI has important implications toward the late-cycle stability of the negative electrode, as it leads to decreased porosity of the porous electrode and, in turn, impeded ionic transport throughout the porous electrode. The steady decrease of the overall electrode porosity by extended SEI will amplify concentration polarization and subsequently increase the propensity for lithium plating at high charging rates. The decrease in electrode porosity from large-scale (~100s of nm) SEI growth has been studied by previous authors,[10−15] particularly on graphitic electrodes cycled at high rate, but the wide range of thicknesses reported in the literature has made this hypothesis challenging to verify. Cryo-EM enables unambiguous observation of SEI evolution as the electrode ages, highlighting the need for an effective, well-passivating SEI.

In summary, we use cryo-TEM to observe the evolution of the SEI on the carbonaceous negative electrode as the electrode cycles. A graphical summary of our observations is presented in Figure 5. The initial SEI formed on the first cycle is thin and primarily amorphous, with a length scale consistent with electron tunneling-limited growth. After prolonged cycling, a compact SEI, consisting of inorganic species such as Li_2O embedded in an amorphous matrix, emerges on some particles. Simultaneously, other particles without inorganic species at the carbon interface exhibit large extended SEI deposits as a result of incomplete passivation. This extended SEI is identified to consist of organic alkyl carbonates. The extreme variation in length scales of compact and extended SEI growth indicates the vastly heterogeneous, but concurrent, SEI growth mechanisms within the electrode. Identifying the sources of these heterogeneities may reveal opportunities to reduce the growth of the extended SEI. SEI growth on the extended SEI scale both consumes large amounts of cyclable lithium and contributes to a decrease in porosity, which likely increases the overpotential for lithium-ion transport and the risk of lithium plating. The inorganic crystallites in the compact SEI appear to play a critical role in preventing large extended SEI growths. Controlling the extent of SEI growth will minimize irreversible capacity loss and the risk of lithium plating, which in turn will increase battery lifetime and safety.

■ ASSOCIATED CONTENT

ⓢ Supporting Information

The Supporting Information is available free of charge on the ACS Publications website at DOI: 10.1021/acs.nano-lett.9b01515.

> Methods, calculations of capacity loss and solvent diffusivity, average SEI thicknesses, TEM, SEM, AFM, DEMS, XPS, and EELS characterization of pristine and cycled carbon black electrodes (PDF)

■ AUTHOR INFORMATION

Corresponding Authors

*E-mail: wchueh@stanford.edu.
*E-mail: yicui@stanford.edu.

ORCID ●

William Huang: 0000-0001-8717-5337
Peter M. Attia: 0000-0003-4745-5726
Hansen Wang: 0000-0002-6738-1659
Sara E. Renfrew: 0000-0003-0445-2963
David T. Boyle: 0000-0002-0452-275X
Yuzhang Li: 0000-0002-1502-7869
Martin Z. Bazant: 0000-0002-8200-4501
Bryan D. McCloskey: 0000-0001-6599-2336
William C. Chueh: 0000-0002-7066-3470
Yi Cui: 0000-0002-6103-6352

Author Contributions

W.H. and P.M.A. contributed equally to this work. W.H. and Z.Z. performed electron microscopy. P.M.A. performed electrode synthesis and electrochemical characterization. H.W., S.E.R., and N.J. performed other characterizations. The manuscript was written through contributions of all authors. All authors have given approval to the final version of the manuscript.

Notes

The authors declare no competing financial interest.

■ ACKNOWLEDGMENTS

■ REFERENCES

(1) Peled, E. *J. Electrochem. Soc.* **1979**, *126* (12), 2047.
(2) Arora, P.; White, R. E.; Doyle, M. *J. Electrochem. Soc.* **1998**, *145* (10), 3647.
(3) Aurbach, D. *J. Power Sources* **2000**, *89* (2), 206−218.
(4) Xu, K. *Chem. Rev.* **2004**, *104* (10), 4303−4417.
(5) Verma, P.; Maire, P.; Novák, P. *Electrochim. Acta* **2010**, *55*, 6332−6341.
(6) Etacheri, V.; Marom, R.; Elazari, R.; Salitra, G.; Aurbach, D. *Energy Environ. Sci.* **2011**, *4* (9), 3243.
(7) Xu, K. *Chem. Rev.* **2014**, *114* (23), 11503−11618.
(8) Peled, E.; Menkin, S. *J. Electrochem. Soc.* **2017**, *164* (7), A1703−A1719.
(9) Pinson, M. B.; Bazant, M. Z. *J. Electrochem. Soc.* **2013**, *160* (2), A243−A250.
(10) Sikha, G.; Popov, B. N.; White, R. E. *J. Electrochem. Soc.* **2004**, *151* (7), A1104.
(11) Broussely, M.; Biensan, Ph.; Bonhomme, F.; Blanchard, Ph.; Herreyre, S.; Nechev, K.; Staniewicz, R. J. *J. Power Sources* **2005**, *146* (1−2), 90−96.
(12) Sarasketa-Zabala, E.; Aguesse, F.; Villarreal, I.; Rodriguez-Martinez, L. M.; López, C. M.; Kubiak, P. *J. Phys. Chem. C* **2015**, *119* (2), 896−906.
(13) Frisco, S.; Kumar, A.; Whitacre, J. F.; Litster, S. *J. Electrochem. Soc.* **2016**, *163* (13), A2636−A2640.
(14) Yang, X.-G.; Leng, Y.; Zhang, G.; Ge, S.; Wang, C.-Y. *J. Power Sources* **2017**, *360*, 28−40.
(15) Louli, A. J.; Ellis, L. D.; Dahn, J. R. *Joule* **2019**, *3*, 745.
(16) Andersson, A. M.; Edström, K. *J. Electrochem. Soc.* **2001**, *148* (10), A1100.

(17) Peled, E.; Bar Tow, D.; Merson, A.; Gladkich, A.; Burstein, L.; Golodnitsky, D. *J. Power Sources* **2001**, *97−98*, 52−57.

(18) Naoi, K.; Ogihara, N.; Igarashi, Y.; Kamakura, A.; Kusachi, Y.; Utsugi, K. *J. Electrochem. Soc.* **2005**, *152* (6), A1047.

(19) Kang, S.-H.; Abraham, D. P.; Xiao, A.; Lucht, B. L. *J. Power Sources* **2008**, *175* (1), 526−532.

(20) Xiao, A.; Yang, L.; Lucht, B. L.; Kang, S.-H.; Abraham, D. P. *J. Electrochem. Soc.* **2009**, *156* (4), A318.

(21) Lu, P.; Harris, S. J. *Electrochem. Commun.* **2011**, *13* (10), 1035−1037.

(22) Wang, F.; Graetz, J.; Moreno, M. S.; Ma, C.; Wu, L.; Volkov, V.; Zhu, Y. *ACS Nano* **2011**, *5* (2), 1190−1197.

(23) Nie, M.; Chalasani, D.; Abraham, D. P.; Chen, Y.; Bose, A.; Lucht, B. L. *J. Phys. Chem. C* **2013**, *117* (3), 1257−1267.

(24) Lu, P.; Li, C.; Schneider, E. W.; Harris, S. J. *J. Phys. Chem. C* **2014**, *118* (2), 896−903.

(25) Bülter, H.; Peters, F.; Schwenzel, J.; Wittstock, G. *Angew. Chem., Int. Ed.* **2014**, *53* (39), 10531−10535.

(26) Gauthier, M.; Carney, T. J.; Grimaud, A.; Giordano, L.; Pour, N.; Chang, H.-H.; Fenning, D. P.; Lux, S. F.; Paschos, O.; Bauer, C.; et al. *J. Phys. Chem. Lett.* **2015**, *6* (22), 4653−4672.

(27) Zhuo, Z.; Lu, P.; Delacourt, C.; Qiao, R.; Xu, K.; Pan, F.; Harris, S. J.; Yang, W. *Chem. Commun.* **2018**, *54* (7), 814−817.

(28) Edström, K.; Herstedt, M.; Abraham, D. P. *J. Power Sources* **2006**, *153* (2), 380−384.

(29) Li, Y.; Li, Y.; Pei, A.; Yan, K.; Sun, Y.; Wu, C.-L.; Joubert, L.-M.; Chin, R.; Koh, A. L.; Yu, Y.; et al. *Science* **2017**, *358* (6362), 506−510.

(30) Aurbach, D. *J. Electrochem. Soc.* **1994**, *141* (1), L1.

(31) Peled, E. *J. Electrochem. Soc.* **1997**, *144* (8), L208.

(32) Bryngelsson, H.; Stjerndahl, M.; Gustafsson, T.; Edström, K. *J. Power Sources* **2007**, *174* (2), 970−975.

(33) Schroder, K. W.; Celio, H.; Webb, L. J.; Stevenson, K. J. *J. Phys. Chem. C* **2012**, *116* (37), 19737−19747.

(34) Unocic, R. R.; Sun, X.-G.; Sacci, R. L.; Adamczyk, L. A.; Alsem, D. H.; Dai, S.; Dudney, N. J.; More, K. L. *Microsc. Microanal.* **2014**, *20* (04), 1029−1037.

(35) Lin, F.; Markus, I. M.; Doeff, M. M.; Xin, H. L. *Sci. Rep.* **2015**, *4* (1), 5694.

(36) Wang, X.; Zhang, M.; Alvarado, J.; Wang, S.; Sina, M.; Lu, B.; Bouwer, J.; Xu, W.; Xiao, J.; Zhang, J. G.; et al. *Nano Lett.* **2017**, *17* (12), 7606−7612.

(37) Zachman, M. J.; Tu, Z.; Choudhury, S.; Archer, L. A.; Kourkoutis, L. F. *Nature* **2018**, *560* (7718), 345−349.

(38) Li, Y.; Huang, W.; Li, Y.; Pei, A.; Boyle, D. T.; Cui, Y. *Joule* **2018**, *2* (10), 2167−2177.

(39) Huang, W.; Boyle, D. T.; Li, Y.; Li, Y.; Pei, A.; Chen, H.; Cui, Y. *ACS Nano* **2019**, *13*, 737.

(40) Attia, P. M.; Das, S.; Harris, S. J.; Bazant, M. Z.; Chueh, W. C. *J. Electrochem. Soc.* **2019**, *166* (4), E97−E106.

(41) Das, S.; Attia, P. M.; Chueh, W. C.; Bazant, M. Z. *J. Electrochem. Soc.* **2019**, *166* (4), E107−E118.

(42) Dahn, J. R.; Fong, R.; Spoon, M. J. *Phys. Rev. B: Condens. Matter Mater. Phys.* **1990**, *42* (10), 6424−6432.

(43) Zheng, T.; Reimers, J. N.; Dahn, J. R. *Phys. Rev. B: Condens. Matter Mater. Phys.* **1995**, *51* (2), 734−741.

(44) Stevens, D. A.; Dahn, J. R. *J. Electrochem. Soc.* **2001**, *148* (8), A803.

(45) Xing, L.; Zheng, X.; Schroeder, M.; Alvarado, J.; von Wald Cresce, A.; Xu, K.; Li, Q.; Li, W. *Acc. Chem. Res.* **2018**, *51* (2), 282−289.

(46) Li, D.; Danilov, D.; Zhang, Z.; Chen, H.; Yang, Y.; Notten, P. H. L. *ECS Trans.* **2014**, *62* (1), 1−8.

(47) Tang, M.; Lu, S.; Newman, J. *J. Electrochem. Soc.* **2012**, *159* (11), A1775−A1785.

(48) Liu, T.; Lin, L.; Bi, X.; Tian, L.; Yang, K.; Liu, J.; Li, M.; Chen, Z.; Lu, J.; Amine, K.; et al. *Nat. Nanotechnol.* **2019**, *14* (1), 50−56.

(49) Zhuang, G. V.; Xu, K.; Yang, H.; Jow, T. R.; Ross, P. N. *J. Phys. Chem. B* **2005**, *109* (37), 17567−17573.

(50) Spahr, M. E.; Palladino, T.; Wilhelm, H.; Würsig, A.; Goers, D.; Buqa, H.; Holzapfel, M.; Novák, P. *J. Electrochem. Soc.* **2004**, *151* (9), A1383.

(51) Spahr, M. E.; Buqa, H.; Würsig, A.; Goers, D.; Hardwick, L.; Novák, P.; Krumeich, F.; Dentzer, J.; Vix-Guterl, C. *J. Power Sources* **2006**, *153* (2), 300−311.

(52) Goers, D.; Spahr, M. E.; Leone, A.; Märkle, W.; Novák, P. *Electrochim. Acta* **2011**, *56* (11), 3799−3808.

(53) Bernhard, R.; Metzger, M.; Gasteiger, H. A. *J. Electrochem. Soc.* **2015**, *162* (10), A1984−A1989.

(54) Brown, Z. L.; Jurng, S.; Nguyen, C. C.; Lucht, B. L. *ACS Appl. Energy Mater.* **2018**, *1*, 3057−3062.

(55) Bar-Tow, D. *J. Electrochem. Soc.* **1999**, *146* (3), 824.

(56) Single, F.; Latz, A.; Horstmann, B. *ChemSusChem* **2018**, *11* (12), 1950−1955.

(57) Peled, E.; Golodnitsky, D.; Ulus, A.; Yufit, V. *Electrochim. Acta* **2004**, *50* (2−3), 391−395.

(58) Billone, M. C.; Liu, Y. Y.; Poeppel, R. B.; Routbort, J. L.; Goretta, K. C.; Kupperman, D. S. *J. Nucl. Mater.* **1986**, *141−143* (1), 282−288.

(59) Chen, Y. C.; Ouyang, C. Y.; Song, L. J.; Sun, Z. L. *J. Phys. Chem. C* **2011**, *115* (14), 7044−7049.

(60) Harris, S. J.; Lu, P. *J. Phys. Chem. C* **2013**, *117* (13), 6481−6492.

(61) Cresce, A. v.; Russell, S. M.; Baker, D. R.; Gaskell, K. J.; Xu, K. *Nano Lett.* **2014**, *14* (3), 1405−1412.

(62) Cody, G. D.; Ade, H.; Alexander, C. M. O. D.; Araki, T.; Butterworth, A.; Fleckenstein, H.; Flynn, G.; Gilles, M. K.; Jacobsen, C.; Kilcoyne, A. L. D.; et al. *Meteorit. Planet. Sci.* **2008**, *43* (1−2), 353−365.

(63) Ploehn, H. J.; Ramadass, P.; White, R. E. *J. Electrochem. Soc.* **2004**, *151* (3), A456.

(64) Horstmann, B.; Single, F.; Latz, A. *Curr. Opin. Electrochem.* **2019**, *13*, 61−69.

(65) Soto, F. A.; Ma, Y.; Martinez De La Hoz, J. M.; Seminario, J. M.; Balbuena, P. B. *Chem. Mater.* **2015**, *27* (23), 7990−8000.

(66) Endo, E.; Ata, M.; Sekai, K.; Tanaka, K. *J. Electrochem. Soc.* **1999**, *146* (1), 49.

(67) Tasaki, K.; Goldberg, A.; Lian, J.-J.; Walker, M.; Timmons, A.; Harris, S. J. *J. Electrochem. Soc.* **2009**, *156* (12), A1019.

(68) Tasaki, K.; Harris, S. J. *J. Phys. Chem. C* **2010**, *114* (17), 8076−8083.

(69) Lin, D.; Liu, Y.; Li, Y.; Li, Y.; Pei, A.; Xie, J.; Huang, W.; Cui, Y. *Nat. Chem.* **2019**, *11*, 382.